Contrib Mineral Petrol (2016) 171:63
DOI 10.1007/s00410-016-1276-2

ORIGINAL PAPER

Orthopyroxene survival in deep carbonatite melts: implications for kimberlites

Rebecca S. Stone[1] · **Robert W. Luth**[1]

Received: 15 March 2016 / Accepted: 13 June 2016 / Published online: 23 June 2016

Abstract Kimberlites are rare diamond-bearing volcanic rocks that originate as melts in the Earth's mantle. The original composition of kimberlitic melt is poorly constrained because of mantle and crustal contamination, exsolution of volatiles during ascent, and pervasive alteration during and after emplacement. One recent model (Russell et al. in Nature 481(7381):352–356, 2012. doi:10.1038/nature10740) proposes that kimberlite melts are initially carbonatitic and evolve to kimberlite during ascent through continuous assimilation of orthopyroxene and exsolution of CO_2. In high-temperature, high-pressure experiments designed to test this model, assimilation of orthopyroxene commences between 2.5 and 3.5 GPa by a reaction in which orthopyroxene reacts with the melt to form olivine, clinopyroxene, and CO_2. No assimilation occurs at 3.5 GPa and above. We propose that the clinopyroxene produced in this reaction can react with the melt at lower pressure in a second reaction that produces olivine, calcite, and CO_2, which would explain the absence of clinopyroxene phenocrysts in kimberlites. These experiments do not confirm that assimilation of orthopyroxene for the entirety of kimberlite ascent takes place, but rather two reactions at lower pressures (<3.5 GPa) cause assimilation of orthopyroxene and then clinopyroxene, evolving carbonatitic melts to kimberlite and causing CO_2 exsolution that drives rapid ascent.

Keywords Experimental petrology · Carbonatite · Kimberlite · Orthopyroxene · Assimilation

Introduction

Both the original melt composition of primary kimberlitic melt and the ascent mechanism for kimberlites have been contentious issues in understanding their formation. Kimberlite melts do not quench to glass and are extensively modified by mantle and crustal contamination, exsolution of volatiles, and alteration. Therefore, the original composition of these melts is poorly constrained. Studies have shown that these melts ascend rapidly to the surface, traveling from depths greater than 200 km to the surface within hours (Peslier et al. 2008 and references therein; Nishi et al. 2010), entraining large amounts of mantle material en route. Exsolution of volatiles such as CO_2 has been suggested to cause this rapid ascent by increasing the buoyancy of the ascending magma or by assisting with dyke propagation (Wilson and Head 2007).

A recent model (Russell et al. 2012) provides both a composition for primary kimberlite melt and a mechanism for CO_2 exsolution to drive ascent. Orthopyroxene is the second most abundant mineral in peridotitic mantle, but is nearly absent from the suite of mantle xenocrysts found in kimberlites. Indeed, the few grains that are present show dissolution textures, implying that orthopyroxene is highly unstable in the kimberlite melt (Mitchell 1973, 2008; Russell et al. 2012). Russell et al. (2012) suggest the reason for this instability is because primary kimberlitic melt is carbonatitic, a more SiO_2-undersaturated and volatile-rich

Communicated by Timothy L. Grove.

Electronic supplementary material The online version of this article (doi:10.1007/s00410-016-1276-2) contains supplementary material, which is available to authorized users.

✉ Robert W. Luth
robert.luth@ualberta.ca

[1] C. M. Scarfe Laboratory of Experimental Petrology, Department of Earth and Atmospheric Sciences, University of Alberta, Edmonton, AB T6G 2E1, Canada

melt than kimberlite. Because of the low activity of silica of this melt, orthopyroxene (a SiO_2 rich mineral) is unstable (Mitchell 1973, 2008; Luth 2009). Assimilation of orthopyroxene into the carbonatitic melt causes an increase in the concentration of SiO_2 in the melt, which decreases the solubility of CO_2 (Brey et al. 1991; Brey and Ryabchikov 1994; Brooker et al. 2011; Moussallam et al. 2015, 2016). Exsolution of CO_2 would then drive ascent of the magma (Russell et al. 2012). In their model, assimilation of orthopyroxene and exsolution of CO_2 commences once the melt ascends from its source region, and continues as long as orthopyroxene is not in equilibrium with the melt. It should be noted that the relationship between carbonatitic and kimberlitic melts has a long history (see review in Kamenetsky et al. 2016), so the proposal that the parental melt was carbonatitic was not new.

Russell et al. (2012) tested the viability of their proposed mechanism in experiments at 1000–1200 °C and atmospheric pressure using Na_2CO_3 as the carbonatitic melt. They explicitly state that their sodium carbonate melts are "…an analog for a natural carbonatitic melt that could be parental (i.e., pre-assimilation) to kimberlites" and further emphasize that "the experiments (e.g., conditions, melt compositions, and scales) are not intended to mimic the natural processes exactly, but to illustrate what is possible and how the process may operate during magma transport." In these experiments, orthopyroxene reacted with the melt, causing exsolution of CO_2 and enrichment of the melt in SiO_2. They did not do experiments at higher pressures.

Subsequently, Kamenetsky and Yaxley (2015) studied orthopyroxene interactions with Na_2CO_3 melt at 2.0–5.0 GPa and 1000–1200 °C. They found that orthopyroxene assimilation did occur, but it did not result in the exsolution of CO_2. Instead, at high pressure (5 GPa) it created a silicate–carbonate melt that unmixes at lower pressure to coexisting carbonate and carbonated silicate melts.

Intrigued by the Russell et al. proposal that orthopyroxene assimilation into carbonatitic melts produces CO_2-saturated kimberlitic melts capable of rapid ascent, we investigated assimilation of orthopyroxene at high pressure and temperature, to explore possible reactions during ascent. Rather than use Na_2CO_3 as an analog for the carbonatitic melt, we initially thought to take advantage of previous studies in the model system CaO–MgO–Al_2O_3–SiO_2–CO_2 that had determined the composition of melts at the solidus of carbonated garnet lherzolite at different pressures (e.g., Dalton and Presnall 1998a; Gudfinnsson and Presnall 2005). The advantage of this system is that the melt at the solidus, coexisting with a carbonated garnet lherzolite mineral assemblage, is isobarically invariant (see, e.g., discussion in Dalton and Presnall 1998a) and therefore, the bulk composition of the starting material can be tailored to produce large volumes of melt, which allows for more reliable analysis of the melt composition than is possible with small-volume interstitial melts, especially in systems where quench modification of the melt is an issue. The model system does have the disadvantage, however, of not allowing evaluation of the effects of other constituents, such as FeO, Na_2O, K_2O, or H_2O. In addition, solidi of carbonated lherzolite in this system are ~200 °C higher than in the natural system (Gudfinnsson and Presnall 2005).

Table 1 Compositions of carbonatitic melt starting materials

System	CMAS + CO_2			CMAS + CO_2 + H_2O
Starting composition	DP	K	G	C
P (GPa)	6	10	16.5	6
T (°C)	1380	1550	1700	1400
SiO_2	5.86	10.21	15.26	13.57
Al_2O_3	0.65	0.68	1.16	0.96
MgO	20.89	31.06	36.49	19.42
CaO	28.02	19.23	6.05	21.45
CO_2	44.58	38.82	41.04	34.18
H_2O	–	–	–	10.42

DP Dalton and Presnall (1998a, b) KM14, *K* Keshav and Gudfinnsson (2014) K-10, *G* Ghosh et al. (2014) D025, *C* Girnis et al. (2011) M322

Dalton and Presnall (1998a) showed that the melts at the solidus of carbonated lherzolite in this system were carbonatitic, with SiO_2 between 5.17 and 6.08 wt%, and their (molar) Mg/(Mg + Ca) increased systematically from 0.41 at 3 GPa to 0.56 at 7 GPa. We selected their melt composition from 6 GPa for this study. To explore the possible effects of changing melt composition on the reactivity of orthopyroxene, we also chose a 10 GPa near-solidus melt composition from the study of Keshav and Gudfinnsson (2014), which was more Mg-rich (Mg/(Mg + Ca) = 0.69) and higher in SiO_2 (10.22 wt%). To further vary the melt compositions, we took a near-solidus melt from 16.5 GPa from Ghosh et al. (2014) and a hydrous near-solidus melt from 6 GPa from Girnis et al. (2011). These two melt compositions were simplified to CaO–MgO–Al_2O_3–SiO_2–CO_2(–H_2O), yielding SiO_2 contents and Mg/(Mg + Ca) of 15.26 wt% and 0.89 and 13.57 wt% and 0.56, respectively. The compositions of each melt, and the pressure and temperature conditions they were previously determined to be in equilibrium with a lherzolitic assemblage, are listed in Table 1 (Dalton and Presnall 1998b; Girnis et al. 2011; Ghosh et al. 2014; Keshav and Gudfinnsson 2014).

Most of our experiments were run at lower pressures than those at which these melts had been previously determined to be in equilibrium with a lherzolitic mineral assemblage. This was done to simulate conditions during ascent of such a melt, which is when orthopyroxene should react with the melt according to the model of Russell et al.

(2012), as well as the previous theoretical analysis by Luth (2009). This latter analysis predicted that any melt formed in equilibrium with olivine and orthopyroxene would, upon ascent, become out of equilibrium with orthopyroxene, providing a driving force for orthopyroxene to react with the melt.

Methods

Starting materials

The compositions of all the carbonatite melts used for these experiments are in the $CaO–MgO–Al_2O_3–SiO_2–CO_2 \pm H_2O$ system. For the CO_2 bearing melts, the starting materials were prepared by mixing and grinding SiO_2 (99.95 %), α-Al_2O_3 (99.99 %), $CaCO_3$ (99.95 %), $MgCO_3$, and MgO (99.95 %) in an agate mortar in ethanol. Before mixing, the silicon, aluminum, and magnesium oxides were fired in a tube furnace for 25 h at 1000 °C (Edgar 1973). The calcium carbonate was dried for 5 h at 300 °C. The magnesite used was a natural magnesite from Mt. Brussilhof, British Columbia, Canada (Enggist et al. 2012). The CO_2- and H_2O-bearing starting material was prepared using the same set of oxides, and except instead of using $MgCO_3$ and MgO as sources for MgO and/or CO_2, magnesium carbonate hydroxide pentahydrate ($(MgCO_3)_4 \cdot Mg(OH)_2 \cdot 5H_2O$), was used as a source of MgO, CO_2, and H_2O.

Because we wanted to maintain the CMAS nature of the experiments, we decided to synthesize enstatite for use in these experiments, rather than use natural mantle-derived orthopyroxene like Russell et al. (2012) did. The orthopyroxene was prepared by mixing equimolar amounts of SiO_2 and MgO under ethanol in an agate mortar for 10 min. The mixture was dried in an oven for 10 min at 120 °C and fired in a tube furnace at 1450 °C for 3 days. Afterward, the powdered mixture was cooled, re-ground, re-dried, and then fired again at 1450 °C for 4 more days. The run product was analyzed on a Rigaku Geigerflex Powder Diffractometer, which confirmed enstatite (both clinoenstatite and protoenstatite) formed. Very minor cristobalite and forsterite peaks were also present.

Experimental setup

For experiments at 2.5 GPa, ~10 mg of starting material was packed into a Pt capsule ~5 mm long with an OD of 3 mm; for experiments >2.5 GPa, capsules were prepared from 5-mm-long by 1.5-mm OD Pt tubing. The capsule was weighed before and after welding in order to detect any sample loss during welding. Minor weight loss of 0.05 mg was routinely observed and was attributed to Pt volatilization during welding. Samples that showed >5 % mass loss were discarded.

The experiments at 2.5 GPa used 12.7-mm talc–Pyrex assemblies in a solid-media, piston-cylinder apparatus (Boyd and England 1960) in the C. M. Scarfe Laboratory for Experimental Petrology, University of Alberta. A $W_{95}Re_5–W_{74}Re_{26}$ thermocouple was used to monitor temperature with no correction for pressure effects on emf. The experiment was first pressurized to approximately 80 % of the run pressure before heating the sample. The sample was heated at a rate of 120 °C min^{-1} at a constant pressure, and then, the pressure was brought up to the desired level.

All experiments at >2.5 GPa were run in the USSA-2000 multi-anvil apparatus at the University of Alberta. The sample assemblies used were an 18/11 M high-temperature assembly with ZrO_2 sleeves (7 mm OD, 3 mm ID) encased in a semi-sintered MgO–5 %Cr_2O_3 octahedron as a pressure cell (Walter et al. 1995). A stepped graphite furnace was used, with the sample centered within the assembly using MgO spacers. An MgO sleeve protected the Pt capsule from direct contact with the graphite furnace. The $W_{95}Re_5–W_{74}Re_{26}$ thermocouple was inserted to the top of the Pt capsule axially by an Al_2O_3 four-bore thermocouple ceramic, and no emf correction was used.

Assemblies were inserted into the cavity in the center of eight 32.5-mm edge-length WC cubes with 11-mm triangular truncations. The assemblies were pressurized at room temperature and then heated at a rate of ~30 or ~60 °C/min per hour. The samples were quenched by cutting the power to the assembly, followed by the decompression at ~30 kbar oil pressure/h. Table 2 lists the run conditions used for all experiments.

Analytical methods

Experimental charges were mounted, polished, and analyzed for phase compositions using a JEOL 8900R electron microprobe (EPMA) at the University of Alberta. Silicates were analyzed using a 15-kV accelerating voltage, a 15-nA current, and a focused beam with 30-s counting time on the peak and 15-s counting time on the background. Carbonates were analyzed using a 10-μm beam, although in some cases the beam was focused to 5 μm because of the small grain size. An accelerating voltage of 15 kV and a current of 15 or 10 nA were used for the carbonates. Frank Smith pyrope, Fo_{93} olivine, diopside, dolomite, spinel, anorthite, and MgO were used as standards. Raw count data were reduced to wt% compositions using the Phi-Rho-Z program supplied by JEOL. The resulting data are tabulated in Supplementary Tables 1–3. Backscatter and secondary electron images were taken of the experimental run products to document the textural relationships present. All

Table 2 Experimental conditions and results

Run #	Starting composition	Assembly	Pressure (GPa)	Temp. (°C)	Duration (h)	Results
PC-DP-RS-001	DP melt	12.7 mm	2.5	1450	5	ol (0.05) + sp (<0.01) + melt (0.95)
DPO-RS-002	DP melt (0.69) + opx (0.31)	12.7 mm	2.5	1450	5	ol (0.31) + cpx (<0.01) + melt (0.54) + CO_2 (0.15)
DP-RS-005	DP melt	18/11 M HT	4.5	1500	6	ol (0.10) + sp (0.01) + per (0.01) + melt (0.89)
DPO-RS-004	DP melt (0.87) + opx (0.13)	18/11 M HT	4.5	1500	6	opx (0.18) + grt (<0.01) + melt (0.82)
DPO-RS-005	DP melt (0.87) + opx (0.13)	18/11 M HT	3.5	1400	6	opx (0.18) + grt (<0.01) + melt (0.82)
K-RS-003	K melt	18/11 M HT	4.5	1600	6	ol (0.05) + grt (0.03) + melt (0.92)
KO-RS-001	K melt (0.89) + opx (0.11)	18/11 M HT	4.5	1600	6	mag (0.12) + opx (0.19) + grt (<0.01) + ol (0.17) + melt (0.68)
G-RS-006	G melt	18/11 M HT	4.5	1650	6	opx (0.08) + grt (0.01) + mag (0.31) + melt (0.59)
GO-RS-002	G melt (0.87) + opx (0.13)	18/11 M HT	4.5	1650	6	opx (0.13) + mag (<0.01) + melt (0.87)
C-RS-001	C melt	18/11 M HT	6	1400	24	mag + coes + melt
OPX-RS-001	C melt (0.64) + opx (0.36)	18/11 M HT	6	1400	24	mag + coes + opx + melt
OPX-RS-002	C melt (0.58) + opx (0.42)	18/11 M HT	4	1400	4	opx + melt

Numbers in parentheses are mass fractions added (starting compositions) or calculated by mass balance (results). Mass balance calculations were not possible for the C melt experiments because of the presence of H_2O as well as CO_2. Phase abbreviations: *sp* spinel, *grt* garnet, *ol* olivine, *coes* coesite, *opx* orthopyroxene, *per* periclase, *cpx* clinopyroxene, *mag* magnesite, *melt* carbonatitic melt

images were taken at 15 kV voltage, 15 nA current, and a rastering focused beam.

Results

The backscatter electron images in Fig. 1a, b show a pair of experiments run at 2.5 GPa and 1450 °C. The experiment in Fig. 1a used the DP carbonatite starting composition alone, which produced mostly melt at these experimental conditions. This melt did not quench to glass but to a mass of mostly carbonate crystals with dendritic textures. A few small grains of olivine (Ol) and spinel (Sp) were also present at the edges of the capsule, which are interpreted to be equilibrium phases. The void space present in this experiment is partially a result of plucking, but some may be the result of CO_2 exsolution, possibly during the quench.

Adding 31 wt% orthopyroxene to the carbonatite bulk composition at the same P, T conditions produces carbonatitic melt (q-Melt), olivine (Ol), and clinopyroxene (Cpx) as shown in Fig. 1b. The formation of large vesicles and the bulging of the capsule are interpreted to mean that CO_2 exsolved from the melt during the experiment. None of the initial orthopyroxene remained. Comparing the electron microprobe analyses of the quenched melt from the two experiments, the assimilation of orthopyroxene increased the SiO_2 concentration by ~15 wt% and decreased the CO_2 content by ~13 wt% (Fig. 2 and Supplementary Table 1).

At 3.5 GPa and 1400 °C, and at 4.5 GPa and 1500 °C, orthopyroxene showed no sign of assimilating into this melt composition, and there was no evidence of exsolution of CO_2 (Table 2, Supplementary Table 1). Electron microprobe analyses confirmed that the melts did not increase in SiO_2 nor decrease in CO_2 content in the presence of orthopyroxene (Fig. 2, Supplementary Table 1). Indeed, the calculated amounts of orthopyroxene in the experiments were greater than the amount of orthopyroxene added to the starting material, suggesting that orthopyroxene actually precipitated during the experiment. These higher-pressure experiments were repeated with other carbonatitic melts to ensure that this result was not specific to this particular melt composition (Table 2). In these experiments, we did not observe dissolution of orthopyroxene nor evidence of exsolution of CO_2. One of these sets of paired experiments used a carbonatitic melt with 10 wt% H_2O added is shown in Fig. 1c, d. Although H_2O has been shown to destabilize orthopyroxene (Kushiro 1970), even in this case orthopyroxene continues to be stable in the carbonatitic melt.

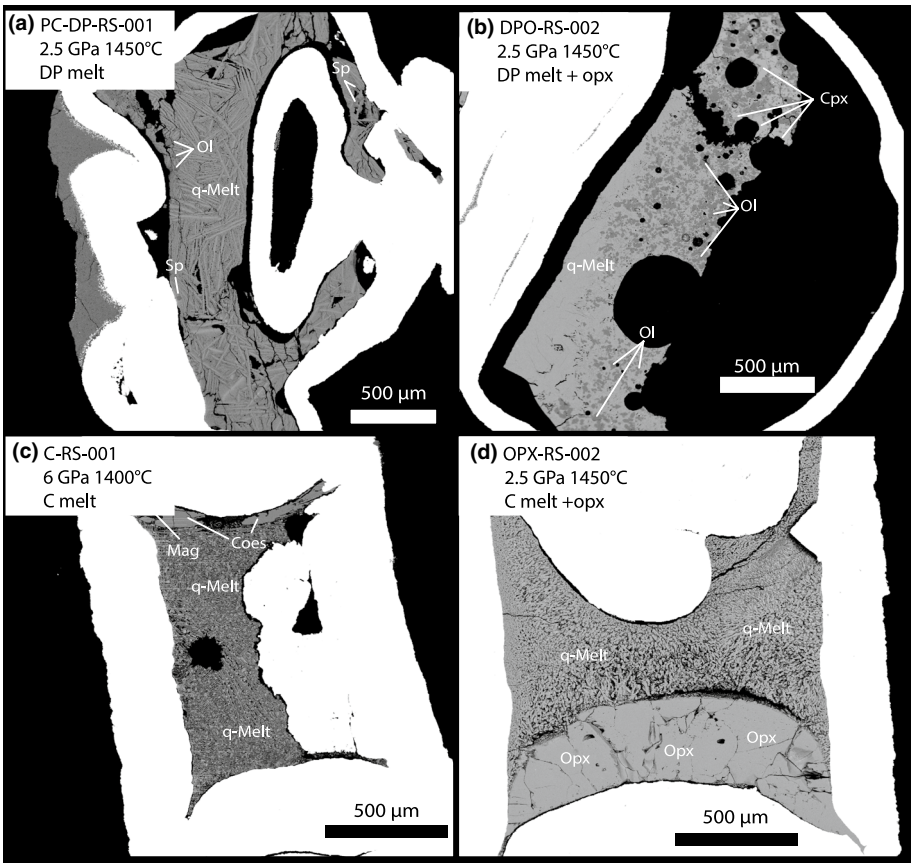

Fig. 1 Backscatter electron images of **a** experiment PC-DP-RS-001 (2.5 GPa, 1450 °C) using the DP carbonatitic melt (see Table 1), **b** experiment DPO-RS-002 (2.5 GPa, 1450 °C) using the DP carbonatitic melt plus 31 wt% orthopyroxene, **c** experiment C-RS-001 (6 GPa, 1400 °C) using the C carbonatitic melt, and **d** experiment OPX-RS-002 (4 GPa, 1400 °C) using the C carbonatitic melt and 42 wt% orthopyroxene. The irregular voids in **c** are a result of plucking the friable quench material and do not represent the presence of fluid during the experiment (in contrast to **b**). *Mag* magnesite, *coes* coesite, *q-Melt* dolomitic carbonatitic melt, *opx* orthopyroxene, *ol* olivine, *cpx* clinopyroxene, *sp* spinel

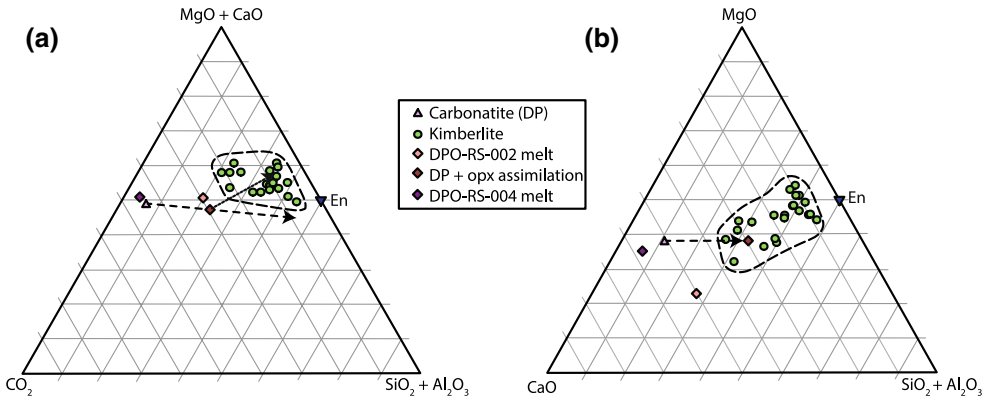

Fig. 2 Ternary plots showing the composition of the DP carbonatite (Table 1), melts compositions from the orthopyroxene-bearing experiments at 2.5 GPa (DPO-RS-002) and 4.5 GPa (DPO-RS-004), and the composition of the DP carbonatite after the assimilation of orthopyroxene and exsolution of CO_2. The *green circles* represent a range of kimberlite compositions from previous studies (Price et al. 2000; Le Roex et al. 2003; Harris et al. 2004; Kjarsgaard et al. 2009; Kopylova et al. 2009; Russell et al. 2012) (Supplementary Table 4). The *dashed line* shows the effect of orthopyroxene assimilation on the composition of the DP carbonatite in the 2.5 GPa experiment, and the *dotted line* shows the effect clinopyroxene assimilation would have at lower pressure

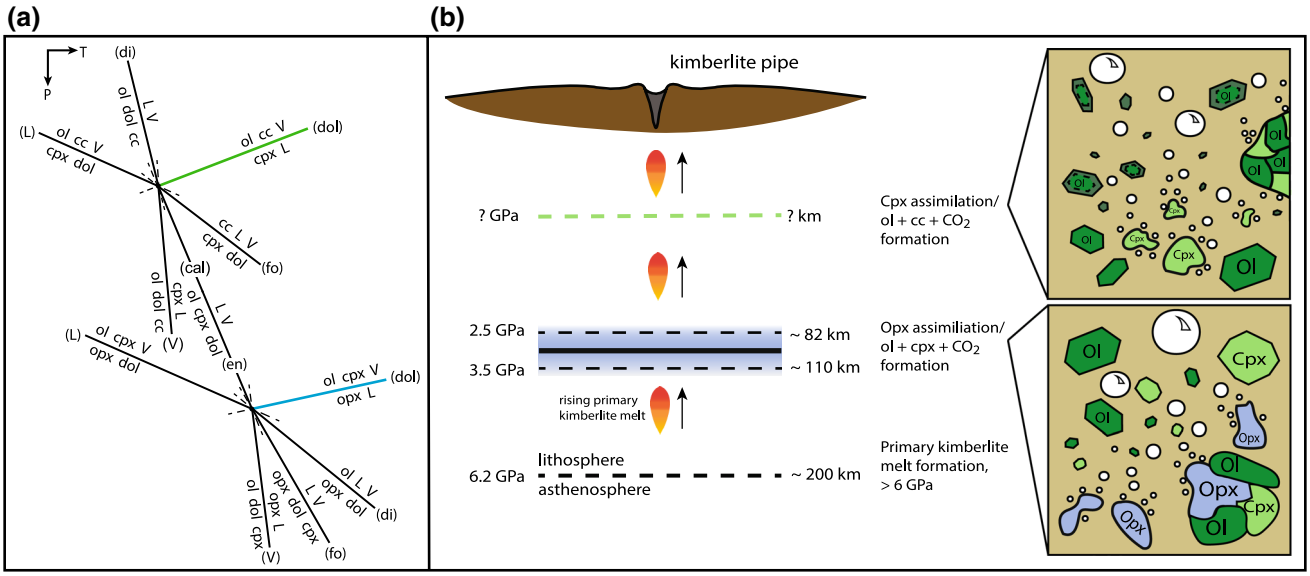

Fig. 3 **a** Schreinemakers' analysis showing the positions of the orthopyroxene (*blue*) and clinopyroxene (*green*) reactions in *P/T* space. Each reaction is labeled with the phase not participating in the reaction, **b** a schematic showing the positions of these reactions with respect to depth and pressure. The *solid black line* represents the pressure (~3 GPa at 1450 °C) that Wyllie and Huang (1976) predicted that orthopyroxene assimilation reaction would occur. In the diagrams showing in the occurring reactions, *blue* represents olivine, *light green* is clinopyroxene, and two different *shades* of *dark green* represent olivine growth due to the two different reactions

Discussion

Formation of clinopyroxene at low pressure

In the 2.5 GPa experiment, the production of clinopyroxene in addition to olivine and CO_2 is consistent with a reaction of the form:

$$2\ Mg_2Si_2O_6(opx) + CaMg(CO_3)_2(melt) \rightarrow 2\ Mg_2SiO_4(ol) + CaMgSi_2O_6(cpx) + 2\ CO_2 \quad (1)$$

taking place. This reaction is the same reaction that forms the "ledge" at ~2.8 GPa in the model lherzolite system $CaO–MgO–SiO_2–CO_2$ (Eggler 1975; Wyllie and Huang 1975a, 1976; Eggler 1978; Moore and Wood 1998; Lee et al. 2000), and the idea that exsolution of CO_2 from ascending carbonatitic and kimberlitic melts upon intersecting this reaction would take place dates back to the 1970s as well (e.g., Wyllie and Huang 1975a, b). The analogous reaction in the $CaO–MgO–Al_2O_3–SiO_2–CO_2$ is of the form:

$$opx + melt = ol + cpx + gt + CO_2 \quad (2)$$

(Dalton and Presnall 1998a; Novella et al. 2014). This reaction lies at lower pressures than does (1), and our run conditions were such that our experiment was above this reaction. Combined with the absence of garnet in our experiment, we believe that reaction (1) better describes our experimental results.

In our 2.5 GPa experiment, the 31 wt% of orthopyroxene originally added was completely consumed, which suggests that the efficacy of the orthopyroxene-consuming reaction is rather high. If the stoichiometry of reaction (1) can be used as a guide, ~68 wt% enstatite would react with a dolomitic carbonatitic melt. The original melt composition in this experiment has molar $Mg/(Ca + Mg) = 0.509$ and low SiO_2 and Al_2O_3 contents, such that it is ~92 wt% $CaMg(CO_3)_2$. Such a melt could consume ~67 wt% orthopyroxene; in other words, the melt can assimilate twice its original mass in orthopyroxene.

Attributing orthopyroxene assimilation to the reaction (1) creates an issue because of the accompanying formation of clinopyroxene. Although common in kimberlite xenocryst suites, clinopyroxene is not a phenocryst phase in kimberlites (Mitchell 1986). If this reaction is the mechanism by which orthopyroxene assimilates in kimberlitic melts, then some subsequent process at lower pressure must eliminate clinopyroxene to explain the absence of phenocrystic clinopyroxene in kimberlite samples. Subsolidus decarbonation reactions can provide some guidance here. As Eggler (1989) noted, there is a lower-pressure decarbonation reaction studied by Käse and Metz (1980) that parallels the sub-solidus analog to reaction (1) and involves clinopyroxene as a reactant:

$$CaMgSi_2O_6(cpx) + 3\ CaMg(CO_3)_2(dol) = 2\ Mg_2SiO_4(ol) + 4\ CaCO_3(cc) + 2\ CO_2 \quad (3)$$

(see also Wyllie and Huang 1976; Wyllie et al. 1983). This suggested that there might be an analogous reaction involving carbonatitic liquid rather than crystalline dolomite and that determining the univariant reactions surrounding the invariant points (ol, opx, cpx, dol, L, V) and (ol, cpx, cc, dol, L, V) in CMS-CO_2 by Schreinemaker's analysis would be a useful exercise. The form of the reactions and their relative positions around each of the invariant points are sensitive to the composition of the liquids involved, but a possible result is shown in Fig. 3a.

The blue line in Fig. 3a is the reaction (1) by which orthopyroxene reacts with the melt. At lower pressure, the reaction:

$$CaMgSi_2O_6(cpx) + 3\ CaMg(CO_3)_2(melt) = 2\ Mg_2SiO_4(ol) + 4\ CaCO_3(cc) + 2\ CO_2 \quad (4)$$

is predicted to occur. The production of CO_2 in this reaction would provide a second burst of volatile exsolution to further accelerate the ascent of the kimberlite. The formation of calcite at the expense of clinopyroxene would also explain the crystallization of primary calcite in kimberlite (Mitchell 2008). A reaction similar to (4) but involving the $CaCO_3$ component of carbonate melt was used by Harmer and Gittins (1997) to explain dolomitic to calcitic carbonatite evolution, but no experimental constraints exist on either variant of this reaction. A recent study looking at clinopyroxene megacrysts (>1 cm in size) in kimberlites found large reaction rims attesting to the instability of clinopyroxene during the ascent of the kimberlite, and crystallized melt inclusions trapped in these megacrysts consist largely of olivine and calcite showing possible evidence of this reaction occurring in nature (Bussweiler et al. 2016).

Melt evolution

Would assimilation of orthopyroxene and clinopyroxene change a carbonatitic melt to a kimberlitic one? Assimilation of orthopyroxene causes the primary carbonatitic melt to increase in SiO_2 content and decrease in CO_2, approaching kimberlitic compositions, but not reaching them with 31 wt% orthopyroxene added (Fig. 2). Assimilation of clinopyroxene would cause more CO_2 exsolution, moving the melt composition along the dotted line (Fig. 2a), into the field of kimberlite compositions. Therefore, it is possible that primary kimberlites are indeed carbonatitic melts as suggested by previous authors (see historical review in Kamenetsky et al. 2016), or possibly a range of carbonatite to transitional melts, that reach kimberlite compositions based on varying amounts of orthopyroxene assimilation, with xenocrystic clinopyroxene also possibly contributing in a secondary manner, which also explains why there is such a large range of kimberlite compositions observed worldwide.

Conclusions

The summary of our model, which builds off the work of Russell et al. (2012), shows that kimberlite ascent at low pressure (less than ~3.5 GPa) is driven by two reactions, one at a pressure between 2.5 and 3.5 GPa and one at an undetermined pressure below 2.5 GPa (Fig. 3b). The first reaction, which is the one that produces the "ledge" in the carbonated peridotite solidus, causes orthopyroxene to assimilate into the carbonatitic melt leading to the crystallization of olivine and clinopyroxene and the production of CO_2, which increases the buoyancy of the melt and drives ascent. Once the melt reaches lower pressures, the clinopyroxene formed in the previous reaction and possibly some xenocrystic clinopyroxene is consumed in the proposed second reaction, forming more olivine and calcite (or possibly a calcite-rich melt). This reaction also produces more CO_2, further accelerating ascent. This crystallization of olivine may contribute to the polybaric olivine assemblage observed in kimberlites (Kamenetsky et al. 2008; Mitchell 2008; Brett et al. 2009; Arndt et al. 2010; Bussweiler et al. 2015; Sobolev et al. 2015) and causes the residual melt to evolve to more CaO-rich compositions which results in calcite later crystallizing as primary groundmass mineral. The consumption of orthopyroxene in the first reaction explains its scarcity in kimberlite samples at the surface. Clinopyroxene xenocrysts and megacrysts may be preserved only because they react at a lower pressure and would stop reacting once the melt becomes too SiO_2 rich. The assimilation of orthopyroxene in the first reaction, the possible contribution of xenocrystic clinopyroxene in the second, and the resulting exsolution of volatiles drive carbonatite compositions to kimberlite before emplacement.

Acknowledgments This project formed part of the M.Sc. research of R.S.S. and was supported by an Natural Sciences and Engineering Research Council Discovery Grant to R.W.L. and funding from the Department of EAS to R.S.S. We acknowledge with thanks technical help by Diane Caird and Andrew Locock and discussions with D.G. Pearson, T. Stachel, and Y. Bussweiler. Constructive and helpful reviews by V. Kamenetsky, J.K. Russell, and an anonymous reviewer are acknowledged with thanks. Their feedback improved this paper, as did the helpful editorial assistance of T. Grove.

References

Arndt NT, Guitreau M, Boullier AM, Le Roex A, Tommasi A, Cordier P, Sobolev A (2010) Olivine, and the origin of kimberlite. J Petrol 51(3):573–602. doi:10.1093/petrology/egp080

Boyd FR, England JL (1960) Apparatus for phase-equilibrium measurements at pressures up to 50 kilobars and temperatures up to 1750 °C. J Geophys Res 65(2):741–748. doi:10.1029/JZ065i002p00741

Brett RC, Russell JK, Moss S (2009) Origin of olivine in kimberlite: phenocryst or impostor? Lithos 112:201–212. doi:10.1016/j.lithos.2009.04.030

Brey GP, Ryabchikov ID (1994) Carbon dioxide in strongly silica undersaturated melts and origin of kimberlite magmas. Neues Jahrb Mineral Monatshefte 10:449–463

Brey GP, Kogarko LN, Ryabchikov ID (1991) Carbon dioxide in kimberlitic melts. Neues Jahrb Mineral Monatshefte 4:159–168

Brooker RA, Sparks RSJ, Kavanagh JL, Field M (2011) The volatile content of hypabyssal kimberlite magmas: some constraints from experiments on natural rock compositions. Bull Volcanol 73(8):959–981. doi:10.1007/s00445-011-0523-7

Bussweiler Y, Foley SF, Prelević D, Jacob DE (2015) The olivine macrocryst problem: new insights from minor and trace element compositions of olivine from Lac de Gras kimberlites, Canada. Lithos 220–223:238–252. doi:10.1016/j.lithos.2015.02.016

Bussweiler Y, Pearson DG, Luth RW, Kjarsgaard BA, Stachel T, Menzies A (2016) The evolution of calcite-bearing kimberlite by rock-melt reaction during ascent: evidence from polymineralic inclusions within Cr-Diopside and Cr-Pyrope megacrysts from Lac de Gras kimberlites, Northwest Territories, Canada. In: GAC-MAC conference, Whitehorse, Yukon

Dalton JA, Presnall DC (1998a) Carbonatitic melts along the solidus of model lherzolite in the system CaO–MgO–Al_2O_3–SiO_2–CO_2 from 3 to 7 GPa. Contrib Mineral Petrol 131:123–135

Dalton JA, Presnall DC (1998b) The continuum of primary carbonatitic-kimberlitic melt compositions in equilibrium with lherzolite: data from the system CaO–MgO–Al_2O_3–SiO_2–CO_2 at 6 GPa. J Petrol 39:1953–1964

Edgar AD (1973) Experimental petrology: basic principles and techniques. Clarendon Press, Oxford

Eggler DH (1975) Peridotite-carbonate relations in the system CaO–MgO–SiO_2–CO_2. Carnegie Inst Wash Year Book 74:468–474

Eggler DH (1978) The effect of CO_2 upon partial melting of peridotite in the system Na_2O–CaO–Al_2O_3–MgO–SiO_2–CO_2 to 35 kb, with an analysis of melting in a peridotite-H_2O–CO_2 system. Am J Sci 278:305–343

Eggler DH (1989) Kimberlites: how do they form? Special publication. Geol Soc Aust 14(2):489–504

Enggist A, Chu L, Luth RW (2012) Phase relations of phlogopite with magnesite from 4 to 8 GPa. Contrib Mineral Petrol 163:467–481. doi:10.1007/s00410-011-0681-9

Ghosh S, Litasov K, Ohtani E (2014) Phase relations and melting of carbonated peridotite between 10 and 20 GPa: a proxy for alkali- and CO_2-rich silicate melts in the deep mantle. Contrib Mineral Petrol. doi:10.1007/s00410-014-0964-z

Girnis AV, Bulatov VK, Brey GP (2011) Formation of primary kimberlite melts—constraints from experiments at 6–12 GPa and variable CO_2/H_2O. Lithos 127(3–4):401–413. doi:10.1016/j.lithos.2011.09.018

Gudfinnsson GH, Presnall DC (2005) Continuous gradations among primary carbonatitic, kimberlitic, melilititic, basaltic, picritic, and komatiitic melts in equilibrium with garnet lherzolite at 3–8 GPa. J Petrol 46(8):1645–1659. doi:10.1093/petrology/egi029

Harmer RE, Gittins J (1997) The origin of dolomitic carbonatites: field and experimental constraints. J Afr Earth Sci 25(1):5–28

Harris M, le Roex A, Class C (2004) Geochemistry of the Uintjiesberg kimberlite, South Africa: petrogenesis of an off-craton, group I, kimberlite. Lithos 74(3–4):149–165

Kamenetsky VS, Yaxley GM (2015) Carbonate–silicate liquid immiscibility in the mantle propels kimberlite magma ascent. Geochim Cosmochim Acta 158:48–56. doi:10.1016/j.gca.2015.03.0k04

Kamenetsky VS, Kamenetsky MB, Sobolev AV, Golovin AV, Demouchy S, Faure K, Sharygin VV, Kuzmin DV (2008) Olivine in the Udachnaya-East kimberlite (Yakutia, Russia): types, compositions and origins. J Petrol 49(4):823–839

Kamenetsky VS et al (2016) Comment on: "The ascent of kimberlite: Insights from olivine" by Brett R.C. et al. [Earth Planet. Sci. Lett. 424 (2015) 119–131]. Earth Planet Sci Lett 440:187–189. doi:10.1016/j.epsl.2016.02.014

Käse H-R, Metz P (1980) Experimental investigation of the metamorphism of siliceous dolomites. Contrib Mineral Petrol 73(2):151–159. doi:10.1007/BF00371390

Keshav S, Gudfinnsson GH (2014) Melting phase equilibria of model carbonated peridotite from 8 to 12 GPa in the system CaO–MgO–Al_2O_3–SiO_2–CO_2 and kimberlitic liquids in the Earth's upper mantle. Am Mineral 99(5–6):1119–1126

Kjarsgaard BA, Pearson DG, Tappe S, Nowell GM, Dowall DP (2009) Geochemistry of hypabyssal kimberlites from Lac de Gras, Canada: comparisons to a global database and applications to the parent magma problem. Lithos 112:236–248. doi:10.1016/j.lithos.2009.06.001

Kopylova MG, Nowell GM, Pearson DG, Markovic G (2009) Crystallization of megacrysts from protokimberlitic fluids: geochemical evidence from high-Cr megacrysts in the Jericho kimberlite. Lithos 112(Supplement 1):284–295. doi:10.1016/j.lithos.2009.06.008

Kushiro I (1970) Systems bearing on melting of the upper mantle under hydrous conditions. Carnegie Inst Wash Year Book 1968–1969:240–245

Le Roex AP, Bell DR, Davis P (2003) Petrogenesis of group I kimberlites from Kimberley, South Africa: evidence from bulk-rock geochemistry. J Petrol 44(12):2261–2286

Lee WJ, Huang WL, Wyllie P (2000) Melts in the mantle modeled in the system CaO–MgO–SiO_2–CO_2 at 2.7 GPa. Contrib Mineral Petrol 138(3):199–213

Luth RW (2009) The activity of silica in kimberlites, revisited. Contrib Mineral Petrol 158(2):283–294. doi:10.1007/s00410-009-0383-8

Mitchell RH (1973) Composition of olivine, silica activity and oxygen fugacity in kimberlite. Lithos 6:65–81

Mitchell RH (1986) Kimberlites: mineralogy, geochemistry, and petrology. Plenum Press, New York

Mitchell RH (2008) Petrology of hypabyssal kimberlites: relevance to primary magma compositions. J Volcanol Geotherm Res 174:1–8

Moore KR, Wood BJ (1998) The transition from carbonate to silicate melts in the CaO–MgO–SiO_2–CO_2 system. J Petrol 39(11–12):1943–1951

Moussallam Y, Morizet Y, Massuyeau M, Laumonier M, Gaillard F (2015) CO_2 solubility in kimberlite melts. Chem Geol 418:198–205. doi:10.1016/j.chemgeo.2014.11.017

Moussallam Y, Morizet Y, Gaillard F (2016) H_2O–CO_2 solubility in low SiO_2-melts and the unique mode of kimberlite degassing and emplacement. Earth Planet Sci Lett 447:151–160. doi:10.1016/j.epsl.2016.04.037

Nishi M, Kubo T, Kato T, Tominaga A, Shimojuku A, Doi N, Funakoshi K-I, Higo Y (2010) Survival of majoritic garnet in diamond by direct kimberlite ascent from deep mantle. Geophys Res Lett. doi:10.1029/2010gl042706

Novella D, Keshav S, Gudfinnsson GH, Ghosh S (2014) Melting phase relations of model carbonated peridotite from 2 to 3 GPa in the system CaO–MgO–Al_2O_3–SiO_2–CO_2 and further indication of possible unmixing between carbonatite and silicate liquids. J Geophys Res Solid Earth 119(4):2780–2800. doi:10.1002/2013jb010913

Peslier AH, Woodland AB, Wolff JA (2008) Fast kimberlite ascent rates estimated from hydrogen diffusion profiles in xenolithic mantle olivines from southern Africa. Geochim Cosmochim Acta 72(11):2711–2722. doi:10.1016/j.gca.2008.03.019

Price SE, Russell JK, Kopylova MG (2000) Primitive magma from the Jericho Pipe, NWT, Canada: constraints on primary kimberlite melt chemistry. J Petrol 41(6):789–808

Russell JK, Porritt LA, Lavallée Y, Dingwell DB (2012) Kimberlite ascent by assimilation-fuelled buoyancy. Nature 481(7381):352–356. doi:10.1038/nature10740

Sobolev NV, Sobolev AV, Tomilenko AA, Kovyazin SV, Batanova VG, Kuz'min DV (2015) Paragenesis and complex zoning of olivine macrocrysts from unaltered kimberlite of the Udachnaya-East pipe, Yakutia: relationship with the kimberlite formation conditions and evolution. Russ Geol Geophys 56(1–2):260–279. doi:10.1016/j.rgg.2015.01.019

Walter MJ, Thibault Y, Wei K, Luth RW (1995) Characterizing experimental pressure and temperature conditions in multi-anvil apparatus. Can J Phys 73(5–6):273–286

Wilson L, Head JW (2007) An integrated model of kimberlite ascent and eruption. Nature 447(7140):53–57

Wyllie PJ, Huang W-L (1975a) Influence of mantle CO_2 in the generation of carbonatites and kimberlites. Nature 257(5524):297–299

Wyllie PJ, Huang WL (1975b) Peridotite, kimberlite, and carbonatite explained in the system CaO–MgO–SiO_2–CO_2. Geology 3(11):621–624

Wyllie PJ, Huang WL (1976) Carbonation and melting reactions in the system CaO–MgO–SiO_2–CO_2 at mantle pressures with geophysical and petrological applications. Contrib Mineral Petrol 54(2):79–107

Wyllie PJ, Huang WL, Otto J, Byrnes AP (1983) Carbonation of peridotites and decarbonation of siliceous dolomites represented in the system CaO–MgO–SiO_2–CO_2 to 30 kbar. Tectonophysics 100(1–3):359–388